

# Charge-stripe crystal phase in an insulating cuprate

He Zhao<sup>1</sup>, Zheng Ren<sup>1</sup>, Bryan Rachmilowitz<sup>1</sup>, John Schneeloch<sup>2</sup>, Ruidan Zhong<sup>2</sup>, Genda Gu<sup>2</sup>, Ziqiang Wang<sup>1</sup> and Ilija Zeljkovic<sup>1\*</sup>

**High-temperature (high- $T_c$ ) superconductivity in cuprates arises from carrier doping of an antiferromagnetic Mott insulator. This carrier doping leads to the formation of electronic liquid-crystal phases<sup>1</sup>. The insulating charge-stripe crystal phase is predicted to form when a small density of holes is doped into the charge-transfer insulator state<sup>1–3</sup>, but this phase is yet to be observed experimentally. Here, we use surface annealing to extend the accessible doping range in Bi-based cuprates and realize the lightly doped charge-transfer insulating state of the cuprate  $\text{Bi}_2\text{Sr}_2\text{CaCu}_2\text{O}_{8+x}$ . In this insulating state with a charge transfer gap on the order of  $\sim 1\text{eV}$ , our spectroscopic imaging scanning tunnelling microscopy measurements provide strong evidence for a unidirectional charge-stripe order with a commensurate  $4a_0$  period along the Cu–O–Cu bond. Notably, this insulating charge-stripe crystal phase develops before the onset of the pseudogap and formation of the Fermi surface. Our work provides fresh insight into the microscopic origin of electronic inhomogeneity in high- $T_c$  cuprates.**

Uncovering the quantum electronic states connecting the two known phases of the cuprate superconductors—the undoped antiferromagnetic Mott (AFM) insulator with a charge transfer gap and the  $d$ -wave superconductor at sufficiently high carrier doping—has been the central challenge for understanding unconventional superconductivity<sup>4</sup>. The experiments so far have primarily focused on exploring novel forms of electronic order in the pseudogap phase of hole-doped cuprates, before and shortly after the onset of superconductivity. Pioneering scattering studies probing the charge dynamics in La- and Y-based cuprates discovered a static<sup>5–7</sup> as well as fluctuating<sup>8</sup> charge-order phase that is also unidirectional (‘stripe’)<sup>5–9</sup>, in analogy to the electronic liquid-crystal nematic or smectic phases proposed for frustrated phase separation<sup>1</sup>. Experiments on Bi- and Cl-based cuprates also revealed a charge order in the pseudogap phase<sup>10–23</sup>, but whether the order originated in the bidirectional ‘chequerboard’<sup>16,17</sup> or the disorder-pinned stripes<sup>10,18,20,21</sup> remains debated. Moreover, the link between these charge-ordered states and the parent charge-transfer insulator state before the onset of the pseudogap remains poorly understood. A key initial proposal suggested that doping induces an inhomogeneous ground state with a tendency to form periodic charge and spin stripes even in the lightly doped AFM phase<sup>2</sup>, an ordering possibly stabilized by the long-range Coulomb interaction<sup>3</sup>. However, direct evidence for such an insulating stripe crystal phase in the insulating cuprates when the charge transfer gap is on the order of  $\sim 1\text{eV}$  has been challenging to obtain, in large part due to the difficulty in synthesizing and characterizing bulk insulating cuprates at low temperatures<sup>13,24</sup>.

$\text{Bi}_2\text{Sr}_2\text{CaCu}_2\text{O}_{8+x}$  (Bi-2212) is a layered cuprate in which the hole density is controlled by off-stoichiometric (interstitial) oxygen

dopant atoms (Fig. 1a), each expected to contribute approximately two holes to the bulk. As-grown Bi-2212 single crystals tend to be optimally doped (hole density  $p \approx 0.16$  per unit cell) with superconducting transition temperature  $T_c \approx 91\text{K}$ . To lower  $p$ , these samples can be subsequently annealed at high temperature in ultrahigh vacuum (UHV) to remove a fraction of oxygen dopants from the bulk. Bulk insulating cuprates have, however, been shown to be difficult to characterize via tunnelling techniques due to there being insufficient charge carriers available for tunnelling<sup>13,24</sup>. Here, we circumvent this problem by demonstrating that a short cycle of annealing in UHV can lead to a significant decrease in the hole density primarily near the exposed topmost surface, while the bulk remains conducting (Supplementary Section 1), providing enough charge carriers for tunnelling experiments. This allows us to use scanning tunnelling microscopy and spectroscopy (STM/S) to study the previously inaccessible insulating state of Bi-2212 at  $\sim 4.5\text{K}$ , in the regime before the charge transfer gap is closed. We find that when only a small density of holes is doped into Bi-2212, an insulating charge-ordered phase arises with commensurate  $4a_0$  unidirectional charge density modulations along the Cu–O–Cu bond (where  $a_0 \approx 3.8\text{Å}$  corresponds to the Bi–Bi, or equivalently Cu–Cu, separation).

We started our experiment by characterizing the surface of UHV-cleaved optimally doped Bi-2212 bulk single crystals ( $T_c \approx 91\text{K}$ ) before any annealing. Consistent with previous reports<sup>25,26</sup>, the  $dI/dV$  spectra (where  $I$  is the current and  $V$  is the voltage applied to the sample) exhibit a spatially inhomogeneous spectral gap, with an average magnitude of  $\Delta_0 \approx 43\text{meV}$  (Fig. 1b). The same sample was then annealed at  $\sim 270^\circ\text{C}$  in UHV (see Methods) and re-inserted into the STM. Although the STM topograph of the post-annealed surface looks qualitatively similar (inset in Fig. 1c), the average  $dI/dV$  spectrum is strikingly different (Fig. 1c). It now shows a V-shape with poorly defined gap-edge peaks (Supplementary Fig. 2), reminiscent of that obtained on underdoped Bi-based cuprates with low but finite  $T_c$  (ref. 15). Interestingly, after annealing the sample at even higher temperature up to  $\sim 380^\circ\text{C}$ , we detected a large insulating gap of  $\Delta_1 \approx 1.1\text{eV}$  in the  $dI/dV$  spectra (Fig. 1d), indicating a transition into the insulating phase (Fig. 1f).

To quantify this process, we used high-bias imaging to visualize the spatial distributions of known oxygen dopants in Bi-2212—‘type-A’ oxygens located near the SrO plane and ‘type-B’ oxygens positioned closer to the BiO layer<sup>27–29</sup>. We found that the densities of both are significantly reduced upon annealing (Fig. 1e and Supplementary Section 2). The annealing process also creates a small number of oxygen vacancies in the SrO layer (Fig. 1e), which are commonly found in underdoped bulk Bi-2212<sup>28</sup>. Based on the concentrations of all oxygen defects, we estimated the hole density of the sample in Fig. 1c to be  $p \approx 0.057 \pm 0.008$  (Supplementary Section 2).

<sup>1</sup>Department of Physics, Boston College, Chestnut Hill, MA, USA. <sup>2</sup>Brookhaven National Laboratory, Upton, NY, USA. \*e-mail: [ilija.zeljkovic@bc.edu](mailto:ilija.zeljkovic@bc.edu)

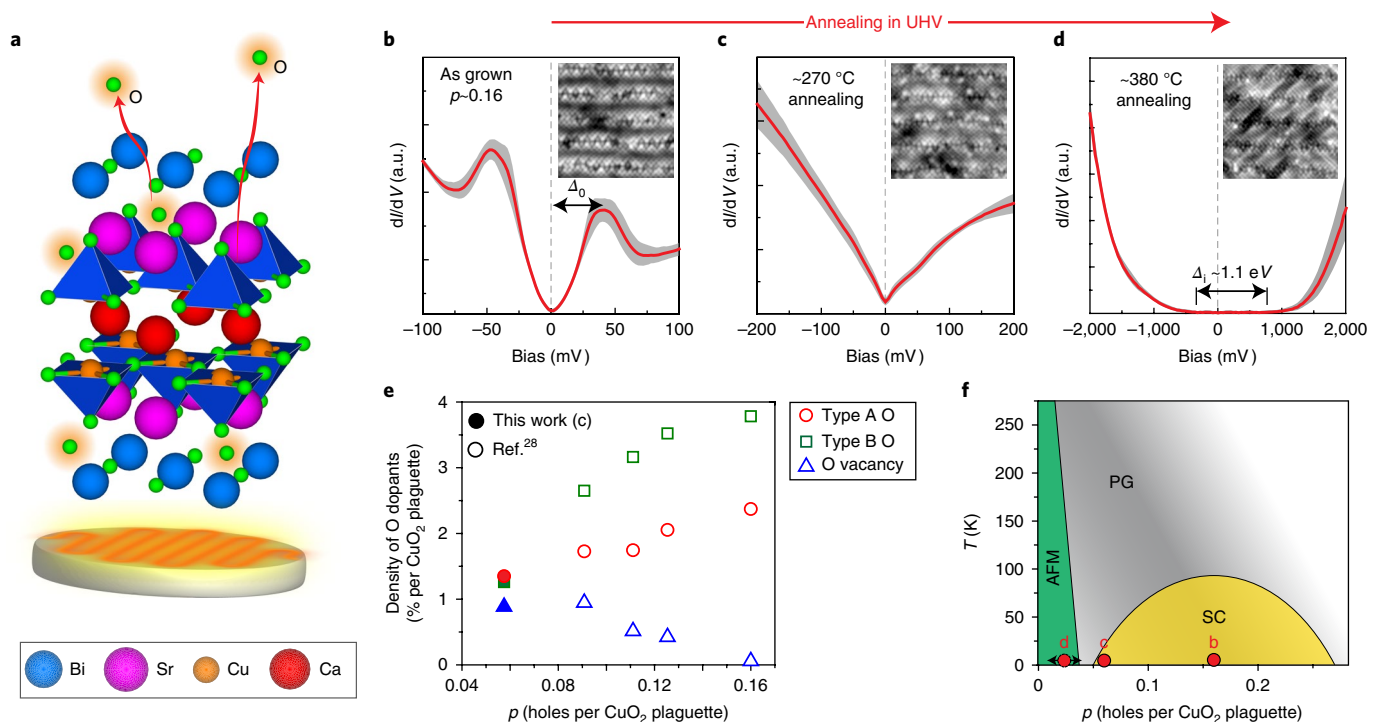


**Fig. 1 | Surface preparation and electronic characterization.** **a**, Schematic of the top half of the Bi-2212 unit cell. Bi-2212 cleaves between two BiO planes to expose a BiO surface, as measured by STM. Annealing removes a fraction of the oxygen atoms, thus reducing the hole density. **b–d**, Average differential conductance ( $dI/dV$ ) spectra acquired on the surface before annealing (**b**), after annealing at  $\sim 270^\circ\text{C}$  (**c**) and after annealing at  $\sim 380^\circ\text{C}$  (**d**). The average spectral gap  $\Delta_0 \approx 43\text{ meV}$  in **b** is calculated as one half of the energy difference between the two gap edge peaks. One half of the width of the grey shaded line at each bias  $V$  represents two standard deviations within  $dI/dV(\mathbf{r}, V)$ , where  $\mathbf{r}$  denotes the lateral position on the sample. Insets in **b–d** are typical STM topographs. **e**, Density of different types of O defects as a function of  $p$ .  $\text{CuO}_2$  plaquette is defined by  $\sim 3.8\text{ \AA}$  square region of each  $\text{CuO}_2$  plane with one Cu atom located in each corner. **f**, Schematic of the hole-doped cuprate phase diagram, with the prominent phases labelled as AFM (antiferromagnetic Mott insulator), SC (superconducting state) and PG (pseudogap). Red circles represent approximate doping levels from **b** and **c**, estimated by counting type A interstitial O atoms, type B interstitial O atoms, and O vacancies, which appear as high-conductance, atomic-scale features in  $dI/dV(\mathbf{r}, V)$  maps acquired at  $-1.5$ ,  $-1$  and  $+1\text{ V}$ , respectively (Supplementary Figs. 4 and 5). The hole density  $p$  in **d** could not be estimated based on the oxygen defect counting (defects could not be unambiguously identified in  $dI/dV(\mathbf{r}, V)$  maps). However, based on the insulating spectra observed, we can schematically represent this data point to be near the AFM transition. STM set-up:  $V_{\text{sample}} = -0.1\text{ V}$ ,  $I_{\text{set}} = 40\text{ pA}$ ,  $V_{\text{exc}} = 4\text{ mV}$  (zero-to-peak) (**b**);  $V_{\text{sample}} = 0.2\text{ V}$ ,  $I_{\text{set}} = 80\text{ pA}$ ,  $V_{\text{exc}} = 5\text{ mV}$  (**c**);  $V_{\text{sample}} = -2\text{ V}$ ,  $I_{\text{set}} = 20\text{ pA}$ ,  $V_{\text{exc}} = 20\text{ mV}$  (**d**).

This is consistent with the average  $V$ -shaped  $dI/dV$  spectrum (Fig. 1c)<sup>15</sup> and the observed incommensurate charge-ordering wavevectors  $\mathbf{Q}^* = 0.28 \pm 0.03$  and  $\mathbf{Q}^{**} = 0.73 \pm 0.04$  (we hereafter define reciprocal lattice vector  $2\pi/a_0 = 1$ ) (Supplementary Fig. 2), all of which are qualitatively similar to those reported in bulk underdoped Bi-2212 with comparable hole density<sup>12,22,23</sup>.

Previous observations of charge ordering in hole-doped cuprates<sup>10–23</sup> have been limited to the approximate doping level achieved in Fig. 1c, in the pseudogap regime with a finite density of states at the Fermi level, after the charge transfer gap has been closed. Now, we turn to characterization of the insulating Bi-2212 surface, which shows a large gap,  $\Delta_s \approx 1.1\text{ eV}$  in the average  $dI/dV$  spectrum at  $\sim 4.5\text{ K}$  (Fig. 1d and Supplementary Fig. 10), comparable to that measured on bulk insulating Bi-2212 at  $\sim 77\text{ K}$  (ref.<sup>24</sup>). The gap is asymmetric with respect to the Fermi level and extends from approximately  $-0.3\text{ eV}$  to  $0.8\text{ eV}$ . A typical STM topograph of the insulating sample, which inevitably contains both the electronic and structural information, clearly shows the individual Bi atoms on the surface as well as the characteristic supermodulation oriented at a  $45^\circ$  angle with respect to the lattice (Fig. 2a). Remarkably, the topograph also exhibits periodic unidirectional features aligned parallel to the Cu–O–Cu lattice direction, which have not been observed before (Fig. 2a). A comparison of reflection high-energy electron diffraction patterns of the pre- and post-annealed surfaces, which

we find to be identical, was used to exclude a structural origin of these modulations (Supplementary Section 3). The spatial extent of unidirectional stripe domains is typically  $\sim 5\text{--}8\text{ nm}$  in length, but it can be as large as a  $\sim 10\text{ nm}$  square region in Fig. 2c, spanning  $>500$  unit cells. Their periodic nature can be confirmed by examining discrete two-dimensional Fourier transforms of the entire STM topograph, where two peaks labelled  $\mathbf{Q}_{\text{CO}}^x$  and  $\mathbf{Q}_{\text{CO}}^y$  emerge at  $(0.25, 0)$  and  $(0, 0.25)$ , respectively (Fig. 2b). These wavevectors suggest that the real-space period of the modulations is exactly  $4a_0$  along either lattice direction. Based on the filtered topograph in Fig. 2e and associated Fourier transform linecuts that show an in-phase relationship between the atomic Bragg peaks  $\mathbf{Q}_x$  and  $\mathbf{Q}_{\text{CO}}^x$  (Fig. 2f), we further conclude that the peaks of the stripe modulation are site-centred, positioned on top of Bi and therefore the Cu sites. This is in contrast to the bond-centred charge modulations observed in underdoped cuprates in the pseudogap regime<sup>18</sup>.

The unidirectional nature of the modulation can be clearly visualized as long horizontal lines that run across the entire field of view (Fig. 2c). Quantitatively, unidirectionality within a single stripe domain can also be confirmed by the presence of only  $\mathbf{Q}_{\text{CO}}^x$  (but not  $\mathbf{Q}_{\text{CO}}^y$ ) in the Fourier transform of the STM topograph (Fig. 2d,f). By constructing the modulation amplitude maps along  $x$  (Fig. 2g) and  $y$  lattice directions (Fig. 2h), we can observe a strong anti-correlation between the two (inset in Fig. 2h), a trend also confirmed for the  $dI/dV(\mathbf{r}, V)$  maps

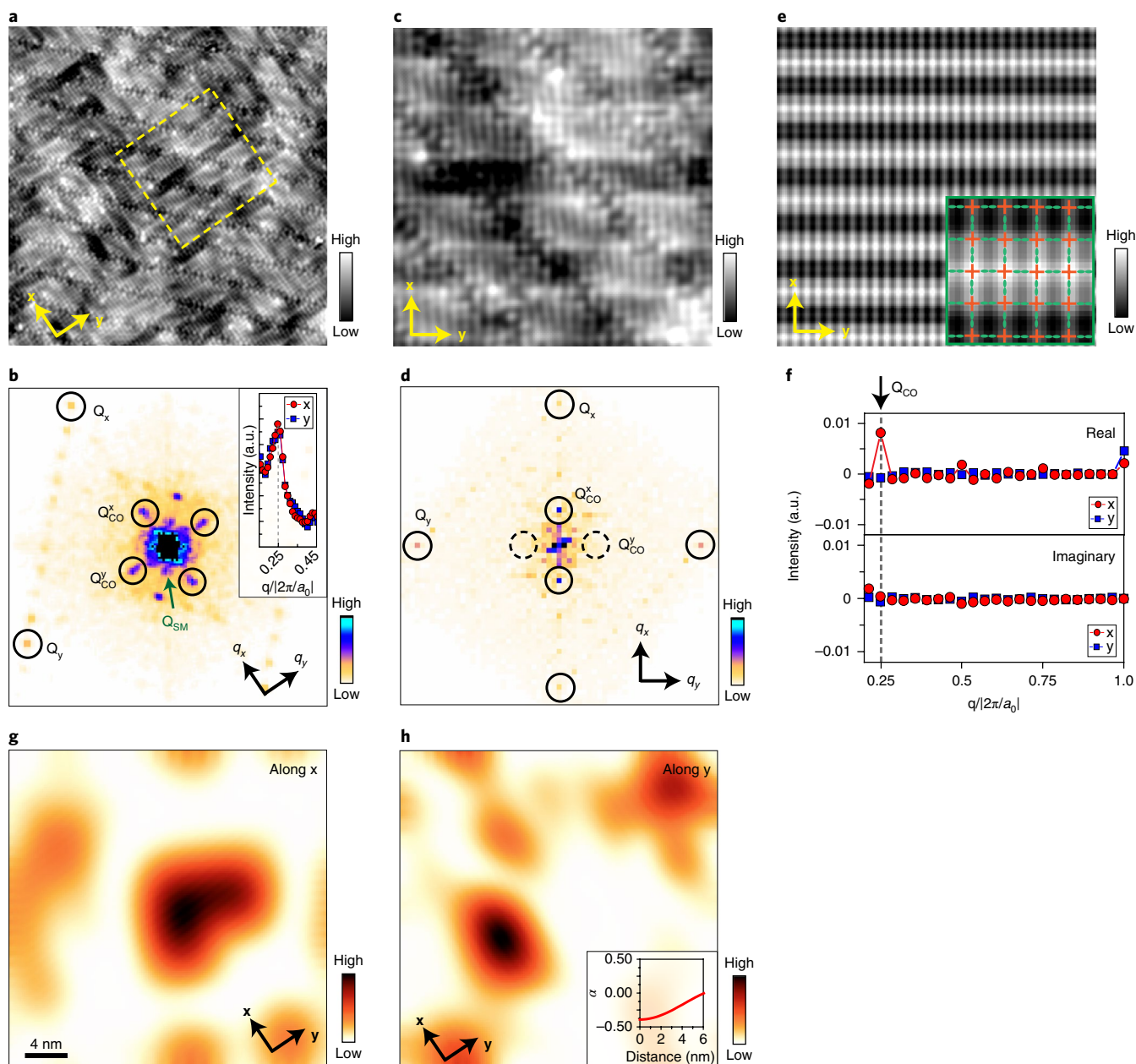


**Fig. 2 | Unidirectional charge-stripe order in insulating Bi-2212.** **a,b**, Atomically resolved STM topograph of a  $\sim 30$  nm square region (**a**) and its associated Fourier transform (**b**). The atomic Bragg peaks ( $Q_x$  and  $Q_y$ ), charge-stripe ordering peaks ( $Q_{CO}^x$  and  $Q_{CO}^y$ ) and the structural supermodulation peak ( $Q_{SM}$ ) are identified. Inset in (**b**), Linecut along  $Q_x$  and  $Q_y$ . **c,d**, Magnified view of a  $\sim 10$  nm square STM topograph hosting a single charge-ordering direction (dashed yellow square in **a**) (**c**) and its associated Fourier transform (**d**). **e**, Fourier-filtered STM topograph from **c** isolating the contributions from wavevectors at  $Q_x$ ,  $Q_y$ ,  $Q_{CO}^x$  and  $Q_{CO}^y$ , only. The topograph demonstrates that the charge order is site-centred. Inset, position of the Cu atoms (orange crosses) and O atoms (green ellipses) in the  $\text{CuO}_2$  layer with respect to the filtered STM topograph. **f**, Linecuts from the centre of the Fourier transform in **d** to  $Q_x$  and  $Q_y$ , showing the real and imaginary Fourier transform components separately. Both  $Q_{CO}^x$  and  $Q_x$  show non-zero real components, while the imaginary components are zero, thus quantitatively confirming their in-phase relationship visually observed in **e, g,h**. The amplitude of the charge-stripe order along **x** (**g**) and **y** (**h**) lattice directions acquired over the region in **a** that show strong anti-correlation with cross-correlation coefficient  $\alpha$  (defined in Supplementary Section 6) of approximately  $-0.4$  (inset in **h**). STM setup (**a,c**):  $V_{\text{sample}} = -2$  V and  $I_{\text{set}} = 3$  pA.

(Supplementary Fig. 8). This is consistent with the visual observation that a certain region of the sample hosts the modulation either along the **x** or **y** lattice direction, but not both. The unidirectional nature cannot be explained by STM tip anisotropy because we observe stripes oriented along both lattice directions using the same tip (Fig. 2a).

We also investigated the electronic origin of this modulation by acquiring  $dI/dV(\mathbf{r}, V)$  maps, where the modulation is visible

as bright lines directly corresponding to the equivalent features observed in the STM topograph (Fig. 3a,b). The associated Fourier transform also shows peaks at  $Q_{CO}^x \sim (0.25, 0)$  and  $Q_{CO}^y \sim (0, 0.25)$  (Fig. 3c), thus demonstrating the ordered nature of the modulations. These modulations are non-dispersive in a wide range of STM biases (Fig. 3d,e), which is consistent with charge ordering. The same ordering vector  $\alpha$  is also seen in normalized  $R(\mathbf{r}, |V|)$

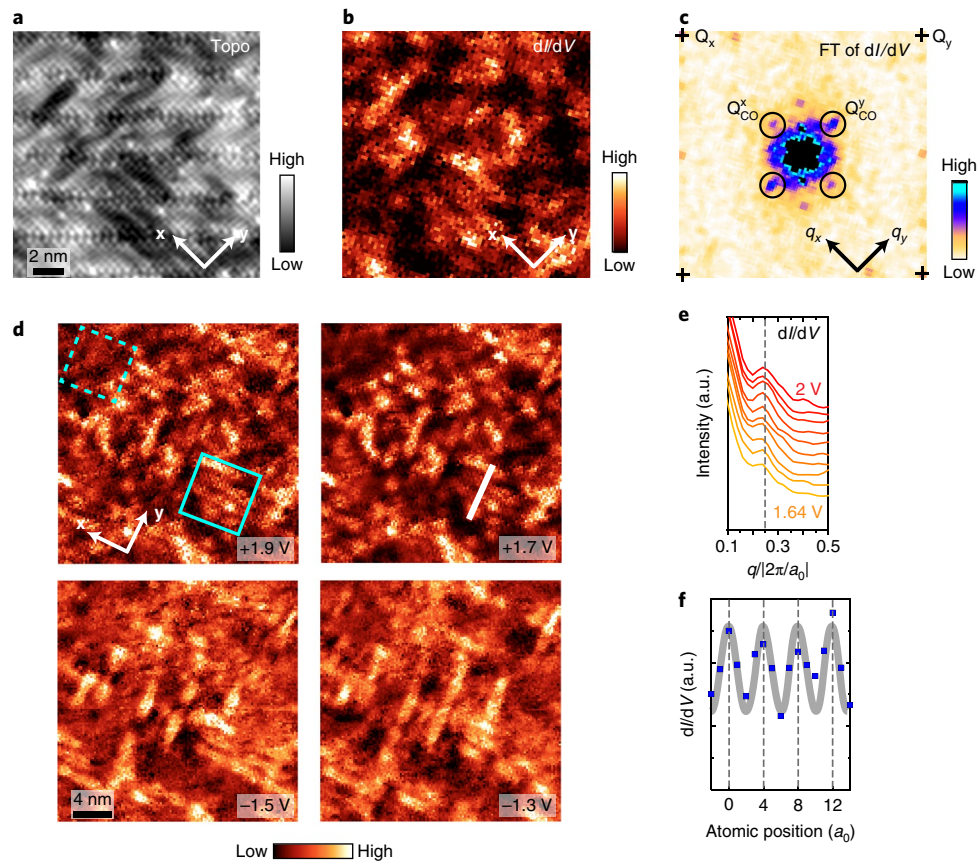


**Fig. 3 | Visualizing the charge-stripe order in STM differential conductance maps of insulating Bi-2212.** **a, b**, Atomically resolved STM topograph (**a**) and  $dI/dV(\mathbf{r}, V=2\text{ V})$  map (**b**) acquired over the same  $\sim 16\text{ nm}$  square region of the sample. **c**, Discrete Fourier transform (FT) of **b** showing  $4a_0$  charge modulation peaks  $Q_{\text{CO}}^x$  and  $Q_{\text{CO}}^y$ . Small crosses in each corner of **c** denote the positions of the atomic Bragg peaks  $Q_x$  and  $Q_y$ . **d**, Four integrated  $dI/dV(\mathbf{r}, V)$  maps at different STM biases acquired over a  $\sim 25\text{ nm}$  square region of the sample. To enhance the signal-to-noise ratio, each map is an average of five  $dI/dV$  conductance maps, spaced by  $40\text{ mV}$ , centred on the bias labelled. **e**, A series of linecuts, offset for clarity, in the four-fold symmetrized Fourier transforms of  $dI/dV(\mathbf{r}, V)$  maps at ten equally spaced biases from  $V=1.64$  to  $2\text{ V}$ . **f**, A real-space linecut along the white line in **d** that shows the periodic variation of the  $dI/dV$  conductance in the  $dI/dV$  map (blue squares), and the ideal  $4a_0$  modulation as a visual guide (grey line). STM set-up:  $V_{\text{sample}} = -2\text{ V}$ ,  $I_{\text{set}} = 20\text{ pA}$  and  $V_{\text{exc}} = 20\text{ mV}$ .

maps used to remove the STM set-up condition<sup>19</sup>. To describe the electronic structure of the striped hole crystal state in more detail, the periodic variation in  $dI/dV(\mathbf{r}, V)$  conductance is shown in Fig. 3f along a linecut across the stripes indicated in Fig. 3d. This modulation in the ordered regions by the  $4a_0$  period can also be seen in the spatial map of the charge transfer gap and its associated Fourier transform (Supplementary Figs. 10 and 11), which is one of the indications suggesting the importance of  $\text{CuO}_2$ -derived Hubbard bands on the physics of the charge-stripe phase (Supplementary Section 4). Our experiments have not been able to pinpoint what type of chemical disorder, if any, could be related to the observed charge modulations. Annealing at the temperatures used in this work is only expected to affect the oxygen dopant density, not the cation concentration<sup>30</sup>. The analysis of oxygen dopant distribution in our surface-annealed samples revealed no spatial ordering with the  $4a_0$  period (Supplementary Section 5). In analogy to the observations in the pseudogap phase of Bi-2212<sup>28</sup>, some correlation between oxygen defects and the maxima/minima of the charge modulations may be possible.

In addition to previously observed smectic<sup>5–10,13,14,18,20,21,23</sup> and nematic<sup>15</sup> orders in the pseudogap phase, we have reported here strong evidence for perhaps the most elusive electron liquid-crystal phase in lightly hole-doped cuprates—the charge-stripe crystal phase. In sharp contrast to the charge-ordered phases in the

pseudogap phase manifested at low energies near the Fermi level, the striped hole crystal phase is detected in the insulating state and is probably tied to the spatial modulations of the high-energy charge transfer gap. Given the long-standing debate on whether the stripes (checkerboard) that break (preserve) the  $C_4$  rotational symmetry of the crystal are favoured in cuprates<sup>31,32</sup>, our work provides real-space evidence that strongly indicates the preference of lightly doped cuprates to form charge stripes over the checkerboard. Our observation of large phase-coherent regions suggests that the striped hole crystal may exist as a stable ground state of a lightly doped Mott insulator stabilized by long-range Coulomb interaction<sup>3</sup>. Moreover, the coexistence of ordered and disordered regions within the same field of view (for example, solid and dashed blue squares in Fig. 3d) could be indicative of Coulomb frustrated phase separation. We further note that the presence of conducting bulk below the insulating surface layers could in principle partially screen the long-range Coulomb interaction in the surface layer (Supplementary Section 1). The observed charge-stripe phase is consistent with the picture of fluctuating stripes<sup>1,33,34</sup> pinned by chemical disorder. We expect it could be detected by resonant X-ray scattering<sup>12,23</sup> provided that the insulating state achieved at the surface by annealing extends into the bulk over micrometre-scale distances. We note that our STM data do not resolve the role of the spin in the observed stripe hole crystal. However, because insulating stripes with both charge and spin order

have been observed in the hole-doped nickelate  $\text{La}_2\text{NiO}_{4+x}$  (ref. <sup>35</sup>), albeit being diagonal and with a much larger charge transfer gap of  $\sim 4\text{eV}$ , it is possible that the insulating charge stripes in Bi-2212 also carry a periodic ordering of spins. Our work provides a viable platform to test this using spin-polarized STM.

Recent experiments have suggested that the charge ordering in cuprates may be intimately related to the pseudogap, and that its wavevector exhibits a doping dependence as if it were driven by Fermi surface effects<sup>36</sup>. However, our data challenge this momentum-space picture, as we provide evidence of a commensurate charge ordering in the charge transfer insulator state, before the onset of the pseudogap and the emergence of a Fermi surface. It is conceivable that the stripe crystal phase serves as the reference insulating state. In this scenario, further hole doping closes the charge transfer gap by nucleating inherently nematic low-energy quasiparticle states, which are unstable to the formation of incommensurate charge and other intertwined orders associated with the pseudogap. This is consistent with a more detailed analysis of STM data, which revealed the underlying commensurate nature of the charge order in the pseudogap phase, disentangled from the apparent incommensurate, doping-dependent vector<sup>14</sup>. However, more experiments are necessary to establish the connections (if any) between the insulating  $4a_0$  stripe hole crystal reported here and the charge-ordering phases in the pseudogap state. Our work provides a promising direction for exploring this by using surface annealing.

### Online content

Any methods, additional references, Nature Research reporting summaries, source data, statements of data availability and associated accession codes are available at <https://doi.org/10.1038/s41563-018-0243-x>.

Received: 4 May 2018; Accepted: 6 November 2018;

Published online: 17 December 2018

### References

- Kivelson, S. A., Fradkin, E. & Emery, V. J. Electronic liquid-crystal phases of a doped Mott insulator. *Nature* **393**, 550–553 (1998).
- Zaenen, J. & Gunnarsson, O. Charged magnetic domain lines and the magnetism of high- $T_c$  oxides. *Phys. Rev. B* **40**, 7391–7394 (1989).
- Löw, U., Emery, V. J., Fabricius, K. & Kivelson, S. A. Study of an Ising model with competing long- and short-range interactions. *Phys. Rev. Lett.* **72**, 1918–1921 (1994).
- Kivelson, S. A. et al. How to detect fluctuating stripes in the high-temperature superconductors. *Rev. Mod. Phys.* **75**, 1201–1241 (2003).
- Tranquada, J. M., Sternlieb, B. J., Axe, J. D., Nakamura, Y. & Uchida, S. Evidence for stripe correlations of spins and holes in copper oxide superconductors. *Nature* **375**, 561–563 (1995).
- Wu, T. et al. Magnetic-field-induced charge-stripe order in the high-temperature superconductor  $\text{YBa}_2\text{Cu}_3\text{O}_y$ . *Nature* **477**, 191–194 (2011).
- Abbamonte, P. et al. Spatially modulated ‘Mottness’ in  $\text{La}_{2-x}\text{Ba}_x\text{CuO}_4$ . *Nat. Phys.* **1**, 155–158 (2005).
- Ghiringhelli, G. et al. Long-range incommensurate charge fluctuations in  $(\text{Y,Nd})\text{Ba}_2\text{Cu}_3\text{O}_{6+x}$ . *Science* **337**, 821–825 (2012).
- Comin, R. et al. Broken translational and rotational symmetry via charge stripe order in underdoped  $\text{YBa}_2\text{Cu}_3\text{O}_{6+y}$ . *Science* **347**, 1335–1339 (2015).
- Howald, C., Eisaki, H., Kaneko, N. & Kapitulnik, A. Coexistence of periodic modulation of quasiparticle states and superconductivity in  $\text{Bi}_2\text{Sr}_2\text{CaCu}_2\text{O}_{8+\delta}$ . *Proc. Natl Acad. Sci. USA* **100**, 9705–9709 (2003).
- Vershinin, M. et al. Local ordering in the pseudogap state of the high- $T_c$  superconductor  $\text{Bi}_2\text{Sr}_2\text{CaCu}_2\text{O}_{8+\delta}$ . *Science* **303**, 1995–1998 (2004).
- Comin, R. et al. Charge order driven by Fermi-arc instability in  $\text{Bi}_2\text{Sr}_{2-x}\text{La}_x\text{Cu}_2\text{O}_{8+\delta}$ . *Science* **343**, 390–392 (2014).
- Cai, P. et al. Visualizing the evolution from the Mott insulator to a charge-ordered insulator in lightly doped cuprates. *Nat. Phys.* **12**, 1047–1051 (2016).
- Mesaros, A. et al. Commensurate  $4a_0$ -period charge density modulations throughout the  $\text{Bi}_2\text{Sr}_2\text{CaCu}_2\text{O}_{8+x}$  pseudogap regime. *Proc. Natl Acad. Sci. USA* **113**, 12661–12666 (2016).
- Lawler, M. J. et al. Intra-unit-cell electronic nematicity of the high- $T_c$  copper-oxide pseudogap states. *Nature* **466**, 347–351 (2010).
- Wise, W. D. et al. Charge-density-wave origin of cuprate checkerboard visualized by scanning tunnelling microscopy. *Nat. Phys.* **4**, 696–699 (2008).

17. Hanaguri, T. et al. A ‘checkerboard’ electronic crystal state in lightly hole-doped  $\text{Ca}_{2-x}\text{Na}_x\text{CuO}_2\text{Cl}_2$ . *Nature* **430**, 1001–1005 (2004).
18. Kohsaka, Y. et al. An intrinsic bond-centered electronic glass with unidirectional domains in underdoped cuprates. *Science* **315**, 1380–1385 (2007).
19. Kohsaka, Y. et al. How Cooper pairs vanish approaching the Mott insulator in  $\text{Bi}_2\text{Sr}_2\text{CaCu}_2\text{O}_{8+\delta}$ . *Nature* **454**, 1072–1078 (2008).
20. Parker, C. V. et al. Fluctuating stripes at the onset of the pseudogap in the high- $T_c$  superconductor  $\text{Bi}_2\text{Sr}_2\text{CaCu}_2\text{O}_{8+x}$ . *Nature* **468**, 677–680 (2010).
21. Kohsaka, Y. et al. Visualization of the emergence of the pseudogap state and the evolution to superconductivity in a lightly hole-doped Mott insulator. *Nat. Phys.* **8**, 534–538 (2012).
22. Fujita, K. et al. Simultaneous transitions in cuprate momentum-space topology and electronic symmetry breaking. *Science* **344**, 612–616 (2014).
23. da Silva Neto, E. H. et al. Ubiquitous interplay between charge ordering and high-temperature superconductivity in cuprates. *Science* **343**, 393–396 (2014).
24. Ruan, W. et al. Relationship between the parent charge transfer gap and maximum transition temperature in cuprates. *Sci. Bull.* **61**, 1826–1832 (2016).
25. Pan, S.-H. et al. Microscopic electronic inhomogeneity in the high- $T_c$  superconductor  $\text{Bi}_2\text{Sr}_2\text{CaCu}_2\text{O}_{8+x}$ . *Nature* **413**, 282–285 (2001).
26. Lang, K. M. et al. Imaging the granular structure of high- $T_c$  superconductivity in underdoped  $\text{Bi}_2\text{Sr}_2\text{CaCu}_2\text{O}_{8+\delta}$ . *Nature* **415**, 412–416 (2002).
27. McElroy, K. et al. Atomic-scale sources and mechanism of nanoscale electronic disorder in  $\text{Bi}_2\text{Sr}_2\text{CaCu}_2\text{O}_{8+\delta}$ . *Science* **309**, 1048–1052 (2005).
28. Zeljkovic, I. et al. Imaging the impact of single oxygen atoms on superconducting  $\text{Bi}_{2+y}\text{Sr}_{2-y}\text{CaCu}_2\text{O}_{8+x}$ . *Science* **337**, 320–323 (2012).
29. Zhou, S., Ding, H. & Wang, Z. Correlating off-stoichiometric doping and nanoscale electronic inhomogeneity in the high- $T_c$  superconductor  $\text{Bi}_2\text{Sr}_2\text{CaCu}_2\text{O}_{8+\delta}$ . *Phys. Rev. Lett.* **98**, 076401 (2007).
30. Mitzi, D. B., Lombardo, L. W., Kapitulnik, A., Laderman, S. S. & Jacowitz, R. D. Growth and properties of oxygen- and ion-doped  $\text{Bi}_2\text{Sr}_2\text{CaCu}_2\text{O}_{8+\delta}$  single crystals. *Phys. Rev. B* **41**, 6564–6574 (1990).
31. Fradkin, E., Kivelson, S. A. & Tranquada, J. M. Colloquium: Theory of intertwined orders in high temperature superconductors. *Rev. Mod. Phys.* **87**, 457–482 (2015).
32. Wang, Y. & Chubukov, A. V. Interplay between unidirectional and bidirectional charge-density-wave orders in underdoped cuprates. *Phys. Rev. B* **92**, 245140 (2015).
33. Arrighoni, E., Fradkin, E. & Kivelson, S. A. Mechanism of high-temperature superconductivity in a striped Hubbard model. *Phys. Rev. B* **69**, 214519 (2004).
34. Huang, E. W. et al. Numerical evidence of fluctuating stripes in the normal state of high- $T_c$  cuprate superconductors. *Science* **358**, 1161–1164 (2017).
35. Tranquada, J. M., Buttrey, D. J., Sachan, V. & Lorenzo, J. E. Simultaneous ordering of holes and spins in  $\text{La}_2\text{NiO}_{4.125}$ . *Phys. Rev. Lett.* **73**, 1003–1006 (1994).
36. Comin, R. & Damascelli, A. Resonant X-ray scattering studies of charge order in cuprates. *Annu. Rev. Condens. Matter Phys.* **7**, 369–405 (2016).

### Acknowledgements

The authors thank M. Allan, J.C. Davis, J.E. Hoffman, S. Kivelson and S. Sachdev for insightful conversations. I.Z. acknowledges support from DARPA grant no. N66001-17-1-4051 (Z.R.), Army Research Office grant no. W911NF-17-1-0399 (B.R.), National Science Foundation grant no. NSF-DMR-1654041 (H.Z.) and the Boston College startup. Z.W. acknowledges support from the US Department of Energy, Basic Energy Sciences grant no. DE-FG02-99ER45747. The work in Brookhaven was supported by the Office of Science, US Department of Energy under contract no. DE-SC0012704. J.S. and R.Z. were supported by the Center for Emergent Superconductivity, an Energy Frontier Research Center funded by the US Department of Energy, Office of Science.

### Author contributions

STM experiments were carried out by H.Z. Magnetization measurements were performed by Z.R. Temperature-dependent reflection high-energy electron diffraction measurements and heater calibration were carried out by B.R. Single crystals of optimally doped Bi-2212 were obtained from J.S., R.Z. and G.G. H.Z. analysed the STM data with guidance from I.Z. I.Z. designed and supervised the project. Z.W. provided theoretical input on the interpretation of STM data. I.Z. and Z.W. wrote the manuscript with input from all the authors.

### Competing interests

The authors declare no competing interests.

### Additional information

Supplementary information is available for this paper at <https://doi.org/10.1038/s41563-018-0243-x>.

Reprints and permissions information is available at [www.nature.com/reprints](http://www.nature.com/reprints).

Correspondence and requests for materials should be addressed to I.Z.

Publisher's note: Springer Nature remains neutral with regard to jurisdictional claims in published maps and institutional affiliations.

© The Author(s), under exclusive licence to Springer Nature Limited 2018

## Methods

The starting point for our experiment is a single crystal of optimally doped Bi-2212 ( $T_c$  of  $\sim 91$  K), grown using the travelling floating zone method. This crystal was cleaved in UHV at room temperature between adjacent BiO layers, and imaged by STM at  $\sim 4.5$  K to demonstrate that the STM topograph and  $dI/dV$  spectra are consistent with previous work (for example, Fig. 1b). The same sample (without re-cleaving) was then taken out of the STM, inserted into the annealing stage in the adjacent UHV chamber, and heated up (annealed) at varying temperatures to achieve the doping levels presented in this Letter. Annealing was performed by the standard procedure for substrate heating also used during molecular beam epitaxy growth. More specifically, heating was achieved by running a current through a heating filament (made from a tungsten wire) inside the sample holder, positioned  $\sim 2$ – $3$  mm behind the sample plate. The temperature of the sample plate was calibrated before and after completion of the STM portion of the experiment in an external UHV chamber, by attaching a thermocouple directly to the top of the sample plate. The sample reached  $\sim 85\%$  of the final temperature within the first  $\sim 5$  min of heating, and the final temperature that the sample reached is reported in the main text. For example, the sample in Fig. 1c was annealed for 10 min to reach a maximum temperature of  $\sim 270^\circ\text{C}$ , and that in Fig. 1d was annealed for three cycles of 20 min each, reaching a maximum of  $\sim 380^\circ\text{C}$  (a single cycle of 20 min heating gave qualitatively the same results). We emphasize again that the sample was never taken out of the UHV environment from the time it was first cleaved until the STM experiments were completed. Annealing at temperatures of  $\sim 430^\circ\text{C}$  (four attempts) yielded an insulating surface that we could not tunnel into at  $\sim 4.5$  K using an STM set-up voltage as high as 3 V and a tunnelling current as low as a few pA, despite no change in room-temperature reflection high-energy electron diffraction images of the surface (Supplementary Figs. 6 and 7). This is consistent with more oxygens escaping from the several topmost layers, which further underdopes the surface, without affecting the structural morphology of the surface.

We note that the bulk of our UHV annealed Bi-2212 samples still exhibit superconductivity, with  $T_c$  reduced by only  $\sim 2$ – $3\%$  (Supplementary Fig. 1), in spite of the dramatic change of the electronic properties at the surface (Fig. 1b–d). Thus, the effects observed here are a consequence of surface doping, possibly of only the several topmost layers where oxygen dopant concentration is significantly reduced. Nevertheless, given the surface-sensitivity of STM, the measurements acquired on this insulating surface are not expected to be affected by the conducting bulk, as further discussed in Supplementary Section 1.

Although difficult to quantify, the rate of oxygen dopants escaping during annealing is probably not a linear function of temperature or the annealing time, as the superconducting bulk acts as an infinite reservoir of oxygen dopants that can partially replace some of the interstitials that escape from the surface. Nevertheless, based on our data regarding the dopant densities and electronic properties of the annealed samples, we can conclude that the surface doping obtained in the end follows the maximum temperature of the annealing used.

All STM data were acquired at a base temperature of  $\sim 4.5$  K. Spectroscopic measurements were taken using a standard lock-in technique at 915 Hz frequency and varying bias excitation as detailed in the figure captions. The STM tips used were home-made, chemically etched tungsten tips annealed to a bright-orange colour in UHV. Tip quality was evaluated on the surface of a single crystal Cu(111) before performing the measurements presented in this Letter. The Cu(111) surface was cleaned by repeated cycles of heating and argon sputtering in UHV before it was inserted into the STM head.

**Code availability.** The computer code used for data analysis is available upon request from the corresponding author.

## Data availability

The data supporting the findings of this study are available upon request from the corresponding author.